Molecular imaging reveals elevated VEGFR-2 expression in retinal capillaries in diabetes: a novel biomarker for early diagnosis

Dawei Sun,[*,†,‡,§,‖,1] Shintaro Nakao,[*,†,‡,§,1] Fang Xie,[*,†,‡,§,‖,1] Souska Zandi,[*,†,‡,§] Abouzar Bagheri,[¶] Mozhgan Rezaei Kanavi,[¶] Shahram Samiei,[#] Zahra-Soheila Soheili,[**] Sonja Frimmel,[*,†,‡,§] Zhongyu Zhang,[*,†] Zsolt Ablonczy,[††] Hamid Ahmadieh,[¶] and Ali Hafezi-Moghadam[*,†,‡,§,2]

*Center for Excellence in Functional and Molecular Imaging, Brigham and Women's Hospital, Boston, Massachusetts, USA; [†]Department of Radiology and [‡]Department of Ophthalmology, Harvard Medical School, Boston, Massachusetts, USA; [§]Angiogenesis Laboratory, Massachusetts Eye and Ear Infirmary, Boston, Massachusetts, USA; [‖]Department of Ophthalmology, Second Affiliated Hospital of Harbin Medical University, Harbin, China; [¶]Ophthalmic Research Center, Shahid Beheshti University of Medical Sciences, Tehran, Iran; [#]Blood Transfusion Research Center, High Institute for Research and Education in Transfusion Medicine, Tehran, Iran; **National Institute of Genetic Engineering and Biotechnology, Tehran, Iran; and [††]Department of Ophthalmology, Medical University of South Carolina, Charleston, South Carolina, USA

ABSTRACT **Diabetic retinopathy (DR) is a microvascular complication of diabetes and a leading cause of vision loss. Biomarkers and methods for early diagnosis of DR are urgently needed. Using a new molecular imaging approach, we show up to 94% higher accumulation of custom designed imaging probes against vascular endothelial growth factor receptor 2 (VEGFR-2) in retinal and choroidal vessels of diabetic animals ($P<0.01$), compared to normal controls. More than 80% of the VEGFR-2 in the diabetic retina was in the capillaries, compared to 47% in normal controls ($P<0.01$). Angiography in rabbit retinas revealed microvascular capillaries to be the location for VEGF-A-induced leakage, as expressed by significantly higher rate of fluorophore spreading with VEGF-A injection when compared to vehicle control (26±2 *vs.* 3±1 μm/s, $P<0.05$). Immunohistochemistry showed VEGFR-2 expression in capillaries of diabetic animals but not in normal controls. Macular vessels from diabetic patients ($n=7$) showed significantly more VEGFR-2 compared to nondiabetic controls ($n=5$) or peripheral retinal regions of the same retinas ($P<0.01$ in both cases). Here we introduce a new approach for early diagnosis of DR and VEGFR-2 as a molecular marker. VEGFR-2 could become a key diagnostic target, one that might help to prevent retinal vascular leakage and proliferation in diabetic patients.—Sun, D., Nakao, S., Xie, F., Zandi, S., Bagheri, A., Kanavi, M. R., Samiei, S., Soheili, Z.-S., Frimmel, S., Zhang, Z., Ablonczy, Z., Ahmadieh, H., Hafezi-Moghadam, A. Molecular imaging reveals elevated VEGFR-2 expression in retinal capillaries in diabetes: a novel biomarker for early diagnosis. *FASEB J.* 28, 3942–3951 (2014). www.fasebj.org**

Key Words: retinopathy · endothelial injury · probe development · preventive care

THE SURGE OF DIABETES is a major problem that both developed and developing countries face today (1). Much of the morbidity and mortality is due to complications in various organs, such as the eye, kidney, brain, or heart. Since generally these complications can be easily prevented if detected early, before irreversible damage is established, biomarkers for subclinical diagnosis are urgently needed.

Diabetic retinopathy (DR), a microvascular complication of diabetes, is the leading cause of adult vision loss. Early DR is characterized by molecular and cellular changes, involving the microvascular endothelium, basement membrane, and pericytes (2, 3). The subsequent proliferative stage involves significant structural changes, such as microaneurysms, obliterating capillaries, and growth of new vessels (4). The new vessels mainly originate from the retinal capillaries (5). The

Abbreviations: ConA, concanavalin A; DR, diabetic retinopathy; MS, microsphere; NPDR, nonproliferative diabetic retinopathy; PDR, proliferative diabetic retinopathy; SLO, scanning laser ophthalmoscope; STZ, streptozotocin; VEGF, vascular endothelial growth factor; VEGFR, vascular endothelial growth factor receptor

[1] These authors contributed equally to this work.

[2] Correspondence: Brigham and Women's Hospital, 221 Longwood Ave., Boston, MA 02115, USA. E-mail: ahm@bwh.harvard.edu

doi: 10.1096/fj.14-251934

This article includes supplemental data. Please visit *http://www.fasebj.org* to obtain this information.

0892-6638/14/0028-3942 © FASEB

mechanisms that underlie the transition from early DR to the proliferative stage remain elusive.

A key molecule in DR pathology is the vascular endothelial growth factor (VEGF)-A, a potent permeability (6) and angiogenic factor. VEGF-A causes proliferation of retinal endothelium by signaling through its cognate receptor, the VEGFR-2 (7). VEGF-A concentration in the eyes of diabetic patients correlates with neovascularization (8), which makes it a therapeutic target (9). However, equally important as VEGF-A itself is the dynamic expression and distribution pattern of VEGFR-2. Recently we showed highest VEGFR-2 expression in the tips of angiogenic vessels, which signals endothelial growth activity (10). However, the dynamics of VEGFR-2 expression in retinal vessels during DR has not been studied in part due to lack of quantitative *in vivo* techniques.

There is currently no method for the evaluation of early molecular changes in the eye. The existing techniques, including angiography and optical coherence tomography, detect tissue changes, such as edema, microaneurysms, or neovascularization. To visualize individual molecules in the retina, we generated molecular imaging probes that bind to endothelial surface molecules (11–14). These probes are systemically injected and their interaction with target endothelial markers visualized by light-based imaging (11, 12). The high sensitivity and specificity of this approach makes it ideal for detection of molecules with very low expression, such as growth factor receptors (12). The noninvasive nature of the imaging approach further allows longitudinal investigations of the expression dynamics of the molecules of interest, something that was not possible with prior end point techniques (15).

VEGF-A signaling through the VEGFR-2 is critical to DR pathology (16); however, the expression and the spatial distribution of the VEGFR-2 in DR is unknown. Using *in vivo* molecular imaging, we contribute new insights about this important molecule in the retinal vessels of diabetic animals and in human histological sections.

MATERIALS AND METHODS

Streptozotocin-induced type 1 diabetes

Male Long-Evans rats (180–200 g, 6–7-wk-old, Charles River Laboratories, Wilmington, MA, USA) were denied access to food overnight and intravenously injected with streptozotocin (STZ, 60 mg/kg, Sigma-Aldrich, St. Louis, MO, USA) diluted in citrate buffer (0.1 M, pH=4.5). Control animals were injected with citrate buffer. Animals were maintained in an air-conditioned room with a 12-h light-dark cycle with free access to water and food. Diabetic status was evaluated by measuring body weight and blood glucose levels. Animals with blood glucose levels higher than 250 mg/dl 24 h after STZ injection were considered diabetic. STZ-injected animals showed significantly higher blood glucose levels and lower body weight compared with the normal controls 2 wk after diabetes induction (**Table 1**).

TABLE 1. *Body weight and blood glucose in normal and diabetic rats*

	Normal rats (n=16)		Diabetic rats (n=17)	
Parameter	d 0	d 14	d 0	d 14
Body weight (g)	177 ± 5	287 ± 11	176 ± 7	188 ± 6**
Blood glucose (mg/dl)	77 ± 9	96 ± 8	74 ± 7	556 ± 43**

Days 0 and 14 refer to the time points after STZ injection in the diabetic groups. Values represent mean ± SEM in each group. **$P <$ 0.01.

This model of hyperglycemia is commonly used in retinal research, though it does not recapitulate important aspects of the human disease (17). For instance, the STZ-treated rats do not show retinal angiogenesis, which is a key cause of severe vision loss in patients with DR. A more realistic model of human disease is the Nile grass rat (18). This spontaneous model of T2D recapitulates all relevant hallmarks of the human metabolic syndrome, *i.e.*, insulin resistance, dyslipidemia, and hypertension (18). The recently characterized retinopathy in these animals shows close resemblance with the human disease and addresses many of the shortcomings of the existing models (19).

Preparation of the molecular imaging probes

Carboxylated fluorescent microspheres (MSs, 2 μm, Polysciences, Warrington, PA, USA) were covalently conjugated to protein G (Sigma-Aldrich), using a carbodiimide-coupling kit (Polysciences) (14). MSs were incubated with nonimmune mouse IgG (mIgG, ctalog no. 0102-14; Southern Biotech, Birmingham, AL, USA), anti-KDR mAb (ab9530; Abcam, KDR/EIC, Cambridge, MA, USA), BSA, or VEGF165 (catalog no. 293/VE/CF; R&D Systems, Minneapolis, MN, USA), for 2 h at room temperature on a rotary shaker and subsequently washed with PBS and BSA (0.1%). Subsequently, MSs were washed again in PBS and sonicated before use *in vivo*. Here 3×10^8 MSs were injected in each animal.

Quantification of molecule number on imaging probes

The average number of α-VEGFR-2 mAb or VEGF molecules on the MS surfaces was determined as described previously (14). Briefly, nonfluorescent MSs (10^6/ml, Polysciences) conjugated to α-VEGFR-2 Ab (mouse-antirat) were incubated with FITC-conjugated goat-anti-mouse IgG or its isotype-matched control (BD Biosciences, Franklin Lakes, NJ, USA) for 30 min or nonfluorescent MSs conjugated to hVEGF-A or albumin and then incubated with rabbit-anti-human VEGF-A Ab for 30 min. After washing with PBS, the MSs were incubated with FITC-conjugated anti-rabbit IgG. Centrifuged at 4000 *g* for 5 min, washed twice, and resuspended into PBS. The fluorescence intensity of 10^4 MSs was measured on a FACScan (Coulter EPICS XL; Beckman Coulter, Fullerton, CA, USA), equipped with the System Work II software.

In parallel, calibration beads (Quantum Simply Cellular; Bangs Laboratories, Fishers, IN, USA) were coated with reference fluorescence antibodies, as described previously (14). Four different populations of MSs with known densities of binding sites for Fc were coated with goat-anti-mouse IgG. Uncoated MSs were used as a control. A calibration curve was generated (R^2=0.99), based on which the average number α-VEGFR-2-Ab or VEGF molecules (27453 and 27094) on the MS surface were determined (Supplemental Fig. S1).

In vivo molecular imaging of retinal and choroidal vessels

To evaluate the number of adherent MSs in the retinal vessels and the choriocapillaris in normal and diabetic animals, a

scanning laser ophthalmoscope (SLO; HRA2; Heidelberg Engineering, Dossenheim, Germany) was used to make continuous high-resolution fundus images. An argon blue laser was used as the excitation light, with a regular emission filter for fluorescein angiography, as the excitation (441nm) and emission (488 nm) maxima of the MSs are comparable with those of sodium fluorescein. After MSs were injected, SLO images were obtained in a 30° angle at 15 frames/s and digitally recorded for further analysis. Images were recorded 30 min after MS injection. The bright spots in SLO micrographs were quantified as a measure for the number of the adherent MSs (Supplemental Fig. 2).

Rats were anesthetized with xylazine hydrochloride (10 mg/kg) and ketamine hydrochloride (50 mg/kg), and their pupils were dilated with 0.5% tropicamide and 2.5% phenylephrine hydrochloride. A contact lens was used to retain corneal clarity throughout the experiment. Conjugated MSs (3×10^8/ml in saline) were continuously injected into the tail vein within 1 min through a 30½ gauge needle. Thirty minutes after the initial injection of the conjugated MSs, the number of free-flowing MSs in the vessels of normal and diabetic rats was substantially diminished, presumably due to the interaction of the MSs with the endothelium of the vessels throughout the body. This allowed us to identify and quantify the number of accumulated MSs in the retinal and choroidal vessels as distinct stationary fluorescent marks with high contrast against the nonfluorescent background. ImageJ software (version 1.41; U.S. National Institute of Health, Bethesda, MD, USA) was used for analysis. For automated quantification of the number of bound MSs in the choriocapillaris microvasculature, the confocal images were merged and subsequently the area of the bright spots measured in ImageJ software.

Ex vivo evaluation of probe binding

Animals were perfused with PBS (pH 7.4) and rhodamine-labeled concanavalin A lectin (RL-1002, Con-A; Vector Laboratories, Burlingame, CA, USA), 10 μg/ml in PBS (pH 7.4). Subsequently 15 ml PBS was injected to wash out excess concanavalin A (ConA). The retina and choroid were microdissected and flatmounted, using a fluorescence antifading medium (Vectashield; Vector Laboratories). The tissues were then observed under an epifluorescence microscope (DM RXA; Leica, Deerfield, IL, USA). Openlab image analysis software (Improvision, Boston, MA, USA) was used to merge images of the MSs (green) with the retinal and the choroidal tissues (red). Microsphere numbers were quantified in each preparation.

Adhesion studies under flow conditions

To investigate the impact of shear on MS adhesion, we performed microfluidic studies under controlled shear conditions (20). Microflow chambers were coated with recombinant VEGFR-2 (5 μg/ml, catalog no. 357-KD/CF; R&D Systems) at 4°C overnight and washed with PBS. Protein-coated chambers were connected to a biocompatible polyester tubing (catalog no. TGY-010-C; Small Parts Inc., Logansport, IN, USA) and a 1 ml syringe filled with conjugated MSs (1×200 dilution compared to animal experiments). With the help of a syringe pump, conjugated MSs were injected through the parallel plate flow chambers. Live videos of the MSs flowing and interacting through the chambers were obtained at 2.5 dyn/cm^2 shear stress at ×10 view for 10 min. The number of adhering MSs was obtained by counting 10 different fields of view at each condition per chamber.

Western blot analysis

Animals were perfused with PBS (500 ml/kg body weight), and eyes were enucleated. Retina and choroid were microsurgically isolated and placed into 150 μl of lysis buffer (mammalian cell lysis kit MCL 1; Sigma-Aldrich), supplemented with protease and phosphatase inhibitors (Sigma-Aldrich), and sonicated. The lysate was centrifuged (12,000 rpm, 15 min, 4°C) and the supernatant was collected. Each sample containing equal amount of total protein, quantified by protein assay (Bio-Rad Laboratories, Richmond, CA, USA) was separated by SDS-PAGE (sodium dodecylsulfate-polyacrylamide gel electrophoresis), and electroblotted to PVDF (polyvinylidene fluoride) membranes (Invitrogen, Carlsbad, CA, USA). Membranes were washed with 5% skim milk and subsequently incubated with a rabbit polyclonal antibody against VEGFR-2 (1:1000, catalog no. 2479; Cell Signaling, Danvers, MA, USA) or a mAb against β-tubulin (1.5 μg/ml; Abcam) at 4°C overnight, followed by incubation with a horseradish peroxidase-conjugated donkey or sheep antibody against rabbit or mouse IgG (1:2000; GE Healthcare UK, Little Chalfont, UK). The signals were visualized with chemiluminescence (ECL kit; GE Healthcare UK) according to the manufacturer's protocol.

Immunohistochemistry

Animals were perfused with Rhodamine ConA and PBS to remove the intravascular content. Retinal flatmounts were fixed (4% paraformaldehyde), washed with PBS, and incubated overnight at 4°C with rabbit anti-mouse VEGFR-2 (5 μg/ml PBS, catalog no. ab9530; Abcam, KDR/EIC). Secondary antibodies included anti-rabbit Ab (Vector Laboratories) and FITC-conjugated Ab (Jackson ImmunoResearch Laboratories, West Grove, PA, USA).

In vivo leakage measurements in rabbit retinal capillaries

Dutch-belted rabbits (1.5 kg; Myrtle's Rabbitry, Thompsons Station, TN, USA) were anesthetized and intravitreally injected with VEGF (100 ng, Sigma-Aldrich) or PBS (10 μl). Two days later high-resolution videos (1 min, 5 frame/s, 1536×1636 pixels) of the early-phase angiographies were taken with a Spectralis HRA-OCT instrument (Heidelberg Engineering, Heidelberg, Germany). For the angiographies, the pupils were dilated with a drop of atropine sulfate (1% solution; Falcon Pharmaceuticals, Fort Worth, TX, USA) and phenylephrine hydrochloride (Akorn, Buffalo Grove, IL, USA). Sterile filtered sodium-fluorescein (2.5 mg/kg; Sigma-Aldrich) was injected intravenously through the marginal ear vein. From the recorded videos, 47 consecutive frames (14–25 s postinjection) were extracted, and 9 successive frames (at 1 s intervals) were selected for image analysis. The presence and spread of fluorescence (fluorescein bubble diameter) at the tips of retina capillaries was measured using Adobe Photoshop CS4 (Adobe Systems, San Jose, CA, USA) and converted to distances using the scale bars on the extracted frames (200 μm/21 pixels). Nine individual retinal areas were selected for quantitation. The rate of bubble diameter increase was determined from linear regressions (Excel 2010; Microsoft, Redmond, WA, USA).

VEGFR-2 in the human retina

After removal of the corneoscleral disc from the whole globe for transplantation purposes, the residual globe was radially incised through the pupillary margin into 4 quadrants. Subsequently, using a magnifying lamp, the retina was evaluated for the presence of hemorrhages, edema, gross neovascularization, or vitreal abnormalities and categorized into 5

groups: no DR, mild nonproliferative DR (NPDR), moderate NPDR, severe NPDR, and proliferative DR (PDR). The eyes that were used in the study were from the mild and moderate NPDR groups. The study did not include eyes that showed more advanced signs of disease, since we were interested in examining the potential of VEGFR-2 as an early diagnostic marker. After staging, the sampling from the macular and peripheral retinal areas was performed. The age of the donors ranged from 48 to 74 yr (60.7±8.03 yr). All eyes were from individuals with type 2 diabetes.

Real-time RT-PCR

Total RNA was extracted using QIAzol Lysis Reagent (Q79306; Qiagen, Hilden, Germany). Concentration and purity of the isolated RNAs were determined using the NanoDrop spectrophotometric analysis. Reverse transcription reaction was performed with QuantiTect Reverse Transcription Kit (205311; Qiagen) and then real-time RT-PCR was performed by a QuantiFast SYBR Green PCR Kit (204054; Qiagen). Primers were GAPDH (QT01192646; Qiagen), B2M (QT00088935; Qiagen), and ACTB (QT01680476; Qiagen) for housekeeping genes and VEGFR-2 (QT00069818; Qiagen). PCR parameters were initial denaturation (one cycle at 95°C for 10 min); denaturation, annealing/amplification for 40 cycles at 95°C for 10 s and 60°C for 30 s, respectively; melting curve, 72°C, with a gradually increasing temperature (0.5°C) to 95°C.

Statistical analysis

All values are expressed as means ± SEM. Data were analyzed by Student's t test. Differences between the experimental groups were considered statistically significant or highly significant, when $P < 0.05$ or $P < 0.01$, respectively.

RESULTS

Increased VEGFR-2 expression in the retina and choroid vessels of diabetic rats

To investigate VEGFR-2 expression in DR, we performed Western blot analysis and immunohistochemistry of VEGFR-2 in retinal and choroidal tissues of normal and diabetic animals (**Fig. 1*A, C***). In the retinal as well as in the choroidal tissues, the ratio of VEGFR-2 to β-tubulin was significantly higher in the diabetic animals (Fig. 1*B, D*).

Normal animals showed low level of background staining for VEGFR-2 in immunohistochemistry. In contrast, the retinal capillaries of the diabetic animals showed significant staining for VEGFR-2 (Fig. 1*E*). Interestingly, in diabetic animals most VEGFR-2 staining was found in capillaries, when compared to the larger retinal vessels. This suggests that the microvascular endothelium is a likely source of VEGFR-2 expression in diabetes.

In vivo molecular imaging of VEGFR-2 in the retina

To quantitatively investigate the expression of VEGFR-2 in the retina, we performed *in vivo* imaging using custom-designed molecular probes (12). Compared to conventional fundus imaging that visualizes the anatomy (**Fig. 2*A***), the new technology provides a discrete signal for expression of the molecules of interest (Fig.

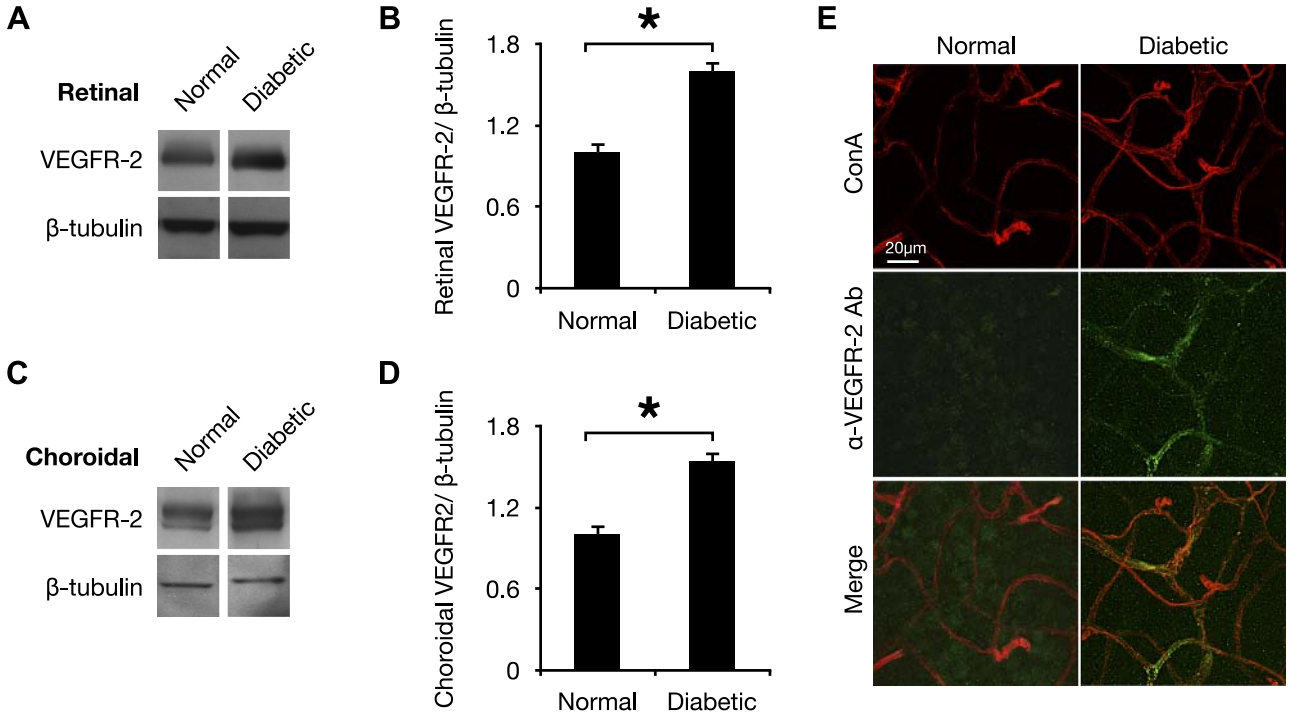

Figure 1. Increased retinal and choroidal VEGFR-2 in experimental diabetes. *A*) Western blot of retinal VEGFR-2 in normal and diabetic animals. *B*) Quantitative analysis of VEGFR-2 and β-tubulin in retinal samples (n=4, each group). *C*) Western blot of choroidal VEGFR-2. *D*) Quantitative analysis of VEGFR-2 in choroidal samples (n=4 in each group). *E*) Immunohistochemistry of VEGFR-2 in perfused retinal vessels in confocal microscopy. Endothelium was stained with rhodamine ConA (red); VEGFR-2 with FITC-conjugated α-VEGFR-2-Ab (green). *$P < 0.05$.

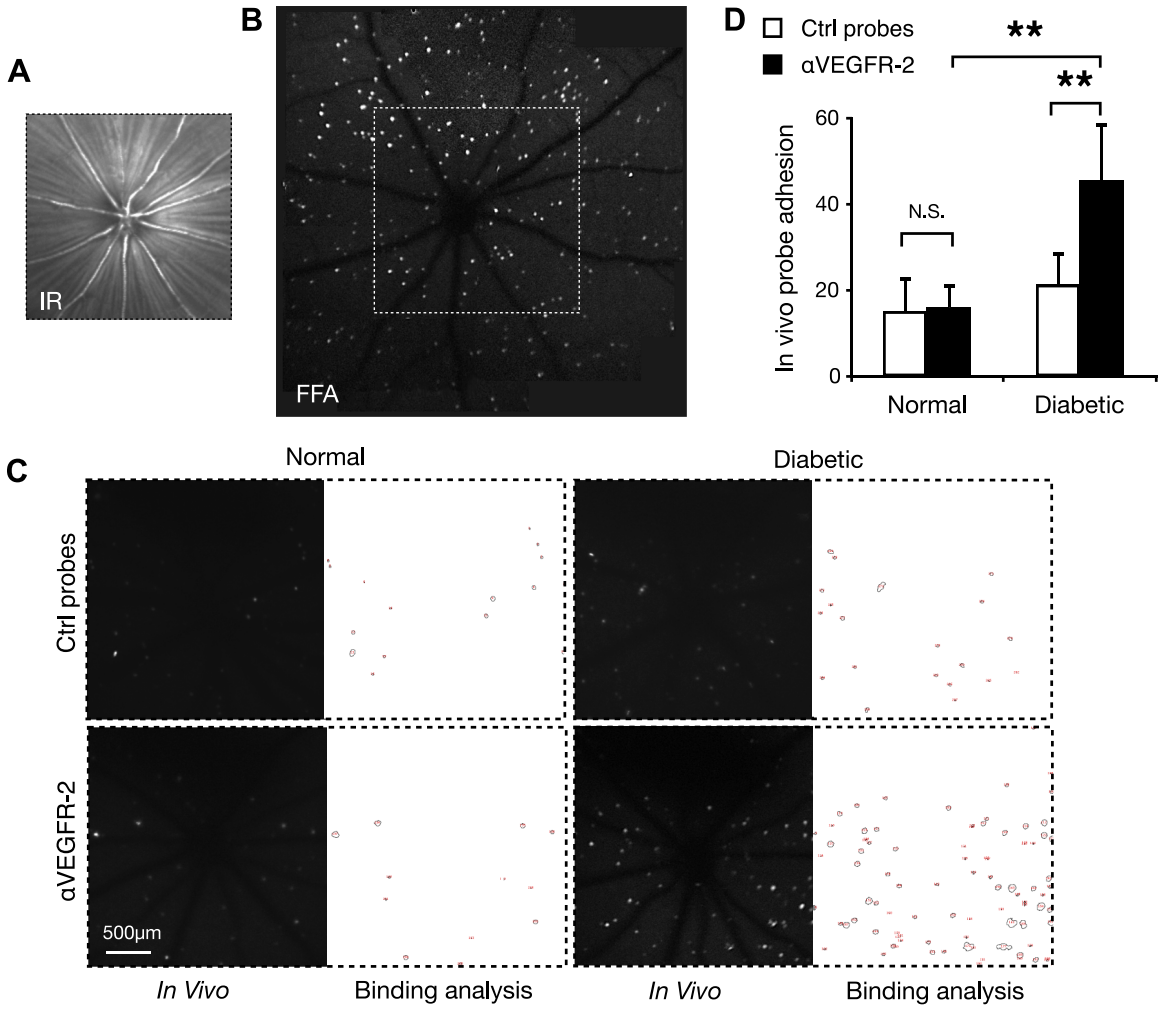

Figure 2. *In vivo* imaging of VEGFR-2 in experimental diabetes. Scanning laser ophthalmoscopy was performed to visualize retinal vessels of normal and diabetic animals. α-VEGFR-2- or IgG-conjugated probes were injected through the tail vein. *A*) Infrared (IR) channel shows the main retinal vessels. *B*) FA channel illustrates a dynamic composite of several fundus regions. White dots indicate adhering αVEGFR-2-conjugated probes in the retinal vasculature. Dashed line, the region of a single field of view, comparable to the IR region. *C*) *In vivo* SLO images and the corresponding automated quantification of accumulated molecular imaging probes in retinal microvessels of diabetic animals. *D*) Quantitative comparison of *in vivo* probe accumulation in normal and diabetic animals, injected with α-VEGFR2- or IgG-conjugated MSs. $n = 5$ in each group. N.S., not significant. $^{**}P < 0.01$.

2*B*). An important distinction from other existing nanoprobes is that our system resolves individual signals that arise from monomolecular interactions. This level of resolution *in vivo* has been unprecedented (12).

In normal animals, α-VEGFR-2- and control IgG-conjugated probes showed low interaction with the retinal endothelium, and there was no significant difference between the 2 groups, as quantified using an automated signal tracking algorithm (Fig. 2*C*). In comparison, in the STZ-injected animals with type 1 diabetes, significantly more α-VEGFR-2-Ab-conjugated probes accumulated, 30 min after injection (Fig. 2*D*).

To validate the *in vivo* results, we generated histological flatmounts. Analogous to the *in vivo* findings, the flatmounts of the diabetic animals injected with α-VEGFR-2 probes showed significantly higher accumulation numbers in retinal vessels (**Fig. 3*A, B***), as well as in the choriocapillaris (Fig. 3*C, D*) than the animals injected with the IgG-conjugated control probes. In the retinal and choriocapillaris vasculature of the normal controls, the binding of the IgG-conjugated MSs did not differ from α-VEGFR2-Ab-conjugated probes.

Leukocytes also express VEGFR-2 and are known to accumulate in the microvasculature of diabetic animals. Therefore, we examined whether the probes directly bind to the microvascular endothelium or also to the accumulated leukocytes. Indeed, 18.4% of the α-VEGFR2 probes were found to bind to the accumulated leukocytes (Fig. 3*E*).

VEGFR-2 distribution in retinal vessels of diabetic animals

Quantification of the distribution of all retinal samples revealed a significantly larger ratio of α-VEGFR-2 probe binding in the capillaries compared to the larger vessels in diabetic animals. The control probes bound at equally low numbers in normal and diabetic animals. In normal animals, there was no significant difference between the distribution of α-VEGFR2-Ab- and IgG-conjugated control probes, while in diabetic animals

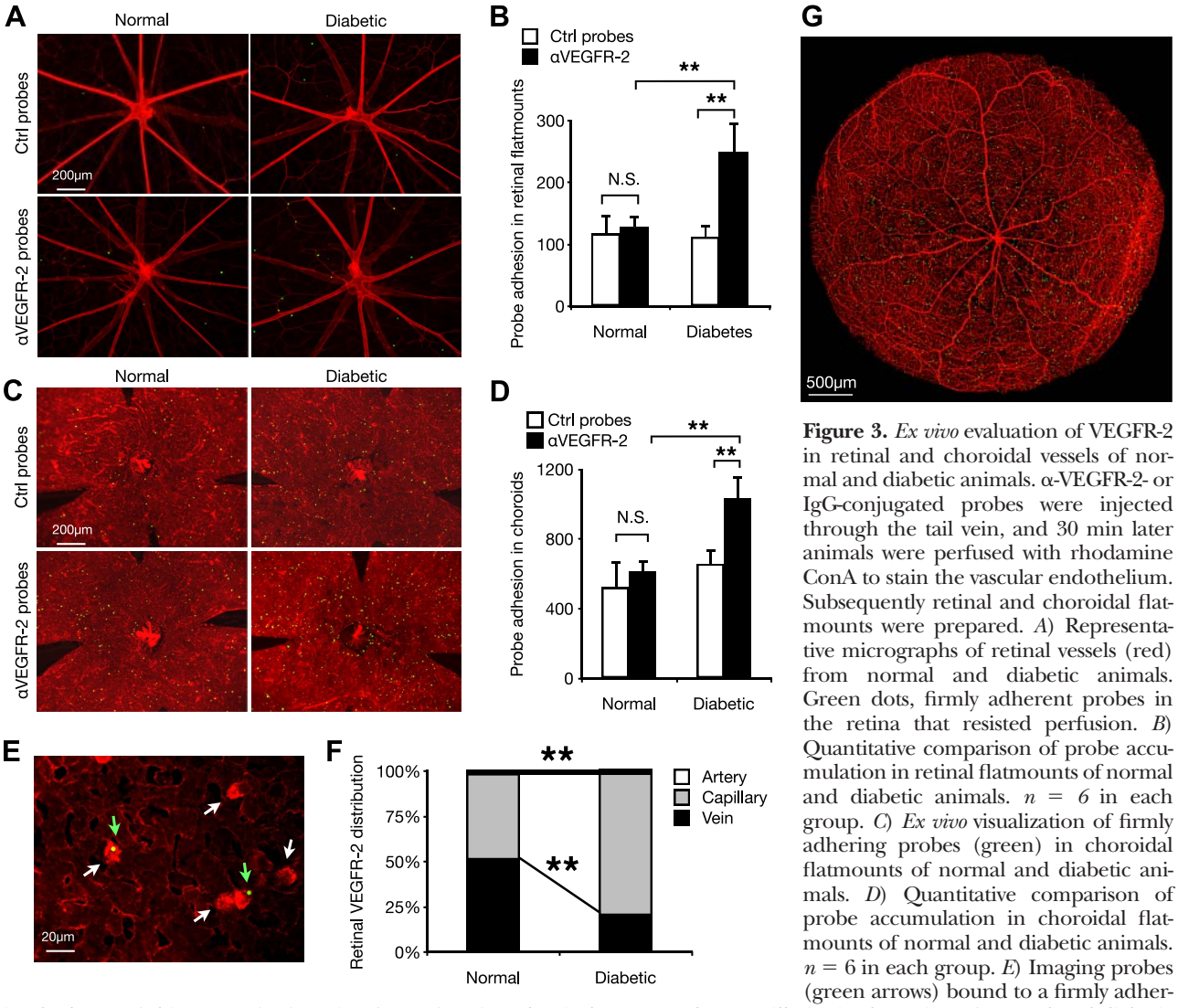

Figure 3. *Ex vivo* evaluation of VEGFR-2 in retinal and choroidal vessels of normal and diabetic animals. α-VEGFR-2- or IgG-conjugated probes were injected through the tail vein, and 30 min later animals were perfused with rhodamine ConA to stain the vascular endothelium. Subsequently retinal and choroidal flatmounts were prepared. *A*) Representative micrographs of retinal vessels (red) from normal and diabetic animals. Green dots, firmly adherent probes in the retina that resisted perfusion. *B*) Quantitative comparison of probe accumulation in retinal flatmounts of normal and diabetic animals. $n = 6$ in each group. *C*) *Ex vivo* visualization of firmly adhering probes (green) in choroidal flatmounts of normal and diabetic animals. *D*) Quantitative comparison of probe accumulation in choroidal flatmounts of normal and diabetic animals. $n = 6$ in each group. *E*) Imaging probes (green arrows) bound to a firmly adhering leukocyte (white arrows). *F*) Ratio of α-VEGFR-2 probes in larger vessels to capillaries in the retina of normal and diabetic animals. $n = 6$ in each group. *G*) A whole retinal flatmount from a diabetic animal, illustrating that the majority of the α-VEGFR-2 probes (green) are in capillaries. N.S., not significant. $^{**}P < 0.01$.

the majority of the probes were found in the capillaries when compared to the larger vessels (Fig. 3*F*). Approximately 1% of the probes bound in the retinal arteries. The micrograph of a whole retinal preparation from a diabetic animal strikingly illustrates that the large majority of the α-VEGFR2 probes accumulated in the capillaries *vs.* in the larger vessels (Fig. 3*G*).

VEGF-A-conjugated imaging probes detect endothelial injury *in vivo*

To facilitate the translation of this molecular imaging approach, we generated VEGF-A coated probes for targeting of the endothelial VEGF receptors. The efficacy of these probes were tested in normal controls and animals with type 1 diabetes (**Fig. 4*A***).

In vivo SLO imaging showed low adhesion numbers for VEGF-A- and albumin-coated control probes in retinal and choroidal vessels in normal animals. In comparison, in diabetic animals significantly more VEGF-A-coated probes adhered to the fundus vessels than control probes (Fig. 4*B*). This provides proof of principle that endogenous growth factors can be used for molecular imaging of their cognate receptors in diabetes.

To examine the location and distribution of the VEGF-A- and albumin-coated probes in the retinal and choriocapillaris vessels, we made histological flatmounts from retinal (Fig. 4*C*) and choroidal (Fig. 4*E*) tissues of normal and diabetic animals. In line with our *in vivo* SLO findings, epifluorescence microscopy showed that most VEGF-A probes accumulated in the retinal (Fig. 4*D*) and choroidal (Fig. 4*F*) capillaries of the diabetic animals.

Adhesion efficacy under physiological shear

To examine the adhesion properties of the VEGF-A and α-VEGFR-2 probes under physiological shear conditions, we performed microfluidic studies. The interaction of the imaging probes with immobilized rVEGFR-2 was visualized by video microscopy under the controlled shear of

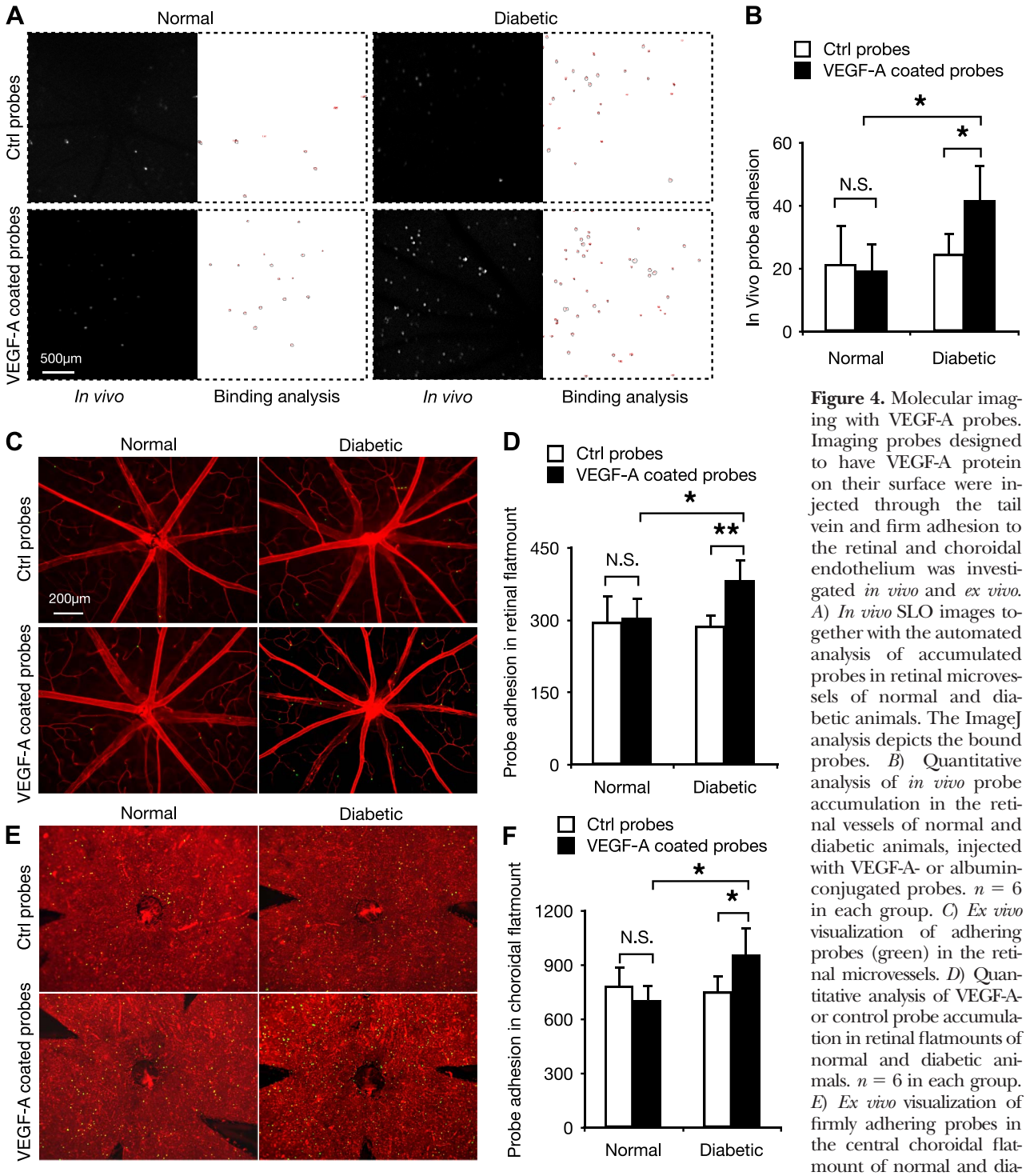

Figure 4. Molecular imaging with VEGF-A probes. Imaging probes designed to have VEGF-A protein on their surface were injected through the tail vein and firm adhesion to the retinal and choroidal endothelium was investigated *in vivo* and *ex vivo*. *A*) *In vivo* SLO images together with the automated analysis of accumulated probes in retinal microvessels of normal and diabetic animals. The ImageJ analysis depicts the bound probes. *B*) Quantitative analysis of *in vivo* probe accumulation in the retinal vessels of normal and diabetic animals, injected with VEGF-A- or albumin-conjugated probes. $n = 6$ in each group. *C*) *Ex vivo* visualization of adhering probes (green) in the retinal microvessels. *D*) Quantitative analysis of VEGF-A- or control probe accumulation in retinal flatmounts of normal and diabetic animals. $n = 6$ in each group. *E*) *Ex vivo* visualization of firmly adhering probes in the central choroidal flatmount of normal and diabetic animals, injected with VEGF-A or control probes. *F*) Quantitative analysis of probe accumulation in choroidal flatmounts of normal and diabetic animals. $n = 6$ in each group. N.S., not significant. $^*P < 0.05$.

2.5 dyn/cm^2 (**Fig. 5*A***) (20). Both α-VEGFR2-Ab- and rVEGF-A-conjugated probes adhered significantly more than the control probes (Fig. 5*B*). Interestingly, α-VEGFR-2 adhesion was higher than VEGF-A probes, likely due to the higher affinity of the antibody to the receptor than VEGF-A. However, the *in vivo* imaging experiments showed that VEGF-A coated probes show sufficient binding. This could be possibly because α-VEGFR-2 exclusively bind the VEGFR-2, whereas VEGF-A also binds the other VEGF receptors, a fact that could compensate for the lower affinity of the probes.

VEGF-A-induced leakage from retinal vascular tips *in vivo*

Next we investigated the location of the VEGF-A-induced vascular leakage by conducting *in vivo* fluorescein angiography with and without intravitreal VEGF-A

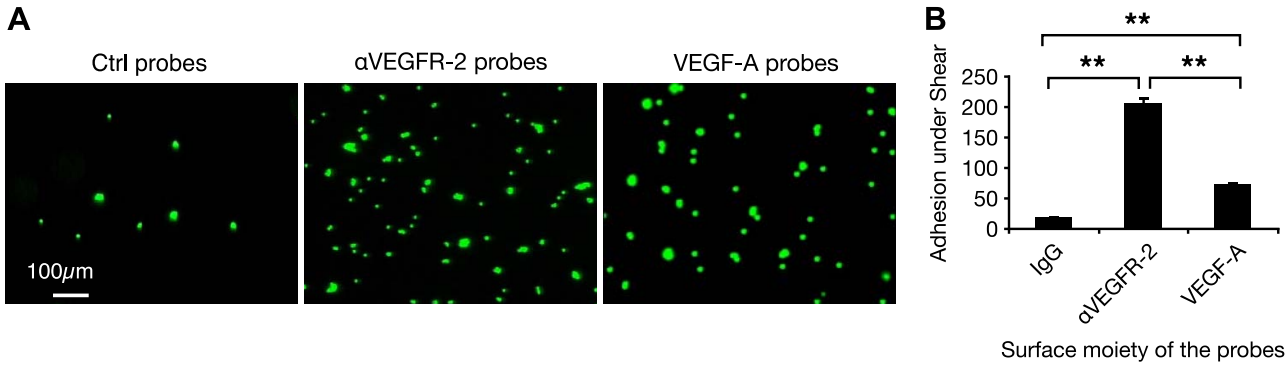

Figure 5. Shear-dependent characteristics of probe accumulation to immobilized VEGFR-2. Parallel plate flow chambers were coated with rVEGFR-2. α-VEGFR-2-, VEGF-A, or control imaging probes were injected through the chamber at a constant rate using a syringe pump and adhesion was evaluated at 2.5 dyn/cm^2 shear stress. *A*) Representative micrographs showing accumulation of α-VEGFR-2-, VEGF-A-, or IgG-conjugated probes onto immobilized VEGFR-2. Green, adherent probes after PBS perfusion. *B*) Quantitative analysis of α-VEGFR-2- or IgG-conjugated probe accumulation in VEGFR-2-coated flow chambers. $n = 10$ in each group. $^{**}P < 0.01$.

injections. For these experiments we chose the rabbit eye, as the rabbit retina is only partially vascularized, which provides a unique opportunity to observe the leakage of capillary tips at the border of the vascularized and the nonvascularized areas. Intravitreal VEGF-A injection caused a previously unreported rapid fluorescein leakage formation around the capillary tips in the early-phase angiographies, indicating a spacially confined reduction in blood-retinal-barrier, while no leakage occurred around the other vessels or in the PBS-injected eyes (**Fig. 6*A***). Quantification of the extravascular fluorescein showed a significantly higher rate of spreading (26±2 μm/s), compared to the PBS-injected (3±1 μm/s) animals (Fig. 6*B*). These results indicate that in normal animals, retinal capillaries are the main location of VEGF-A's action. Since VEGFR-2 is the main endothelial receptor for VEGF-A, the BRB leakage in these experiments might be the equivalent of the capillary VEGFR-2 expression that was found by our molecular imaging.

Higher VEGFR-2 expression in the macula of diabetic patients

To investigate the role of VEGFR-2 in human DR, we obtained retinal tissues from healthy subjects and individuals with type 2 diabetes (average age 60.7±8.03 yr, 60% male). Only eyes with mild or moderate NPDR were included in the examination. Among these eyes, only one eye contained hard exudates. In each retina we performed real-time RT-PCR from the macular tissue as well as the peripheral retinal regions. VEGFR-2 was expressed over 10-fold in the macula of patients with DR compared to the normal nondiabetic controls and was elevated ~4-fold in the periphery (**Fig. 7**). Interestingly, VEGFR-2 was significantly higher in the maculas of the patients with DR compared to the peripheral regions of the retinas of the same patients. For normalization of the results, 3 different housekeeping genes were used, BACT, GAPDH, and B2M, the results of which were comparable in either case. The macular and peripheral increases were 10.78- and 4-fold (BACT), 9.72- and 6-fold (GAPDH), and 7.44- and 2.71-fold (B2M), respectively.

DISCUSSION

Vision loss from DR is preventable with early intervention, yet to date it has not been possible to visualize retinal endothelial injury in patients with diabetes (21). Ideally, early detection of DR would allow treatment before irreversible structural damages occur. Therefore, the need is great to discover biomarkers of early DR and develop realistic strategies for subclinical diagnosis (21).

The eye provides a unique portal for light-based molecular imaging of retinal endothelial surface molecules. To detect VEGFR-2, we generated 2 different imaging probes, one having an αVEGFR-2 mAb and another rVEGF-A as surface moiety. Both probes showed specificity for the target, while the rVEGF-A could also bind to the other VEGF receptors. To prevent side effects of the VEGF-A molecule, a mutated version of the protein that binds to its endothelial receptor but does not cause angiogenesis could be used (22).

Our results showed a higher VEGFR-2 expression in the retinal microvessels of rodents with type 1 diabetes and humans with type 2 diabetes, which could make this molecule a diagnostic target in both types of disease. In the diabetic human retina, the microvessels in the macular region expressed the highest VEGFR-2 levels. Since endothelial VEGFR-2 is a prelude to angiogenesis (10), this could mean a higher susceptibility of the macular microvessels for neovascularization. Using our novel noninvasive molecular imaging approach, we show elevated VEGFR-2 expression in retinal and choroidal vessels of diabetic animals. The *in vivo* data were consistent with the outcome of the established histological flat mounts and Western blotting. Even though, choroidal vessels were not traditionally thought to be involved in the diabetic retinopathy, our results indicate their participation.

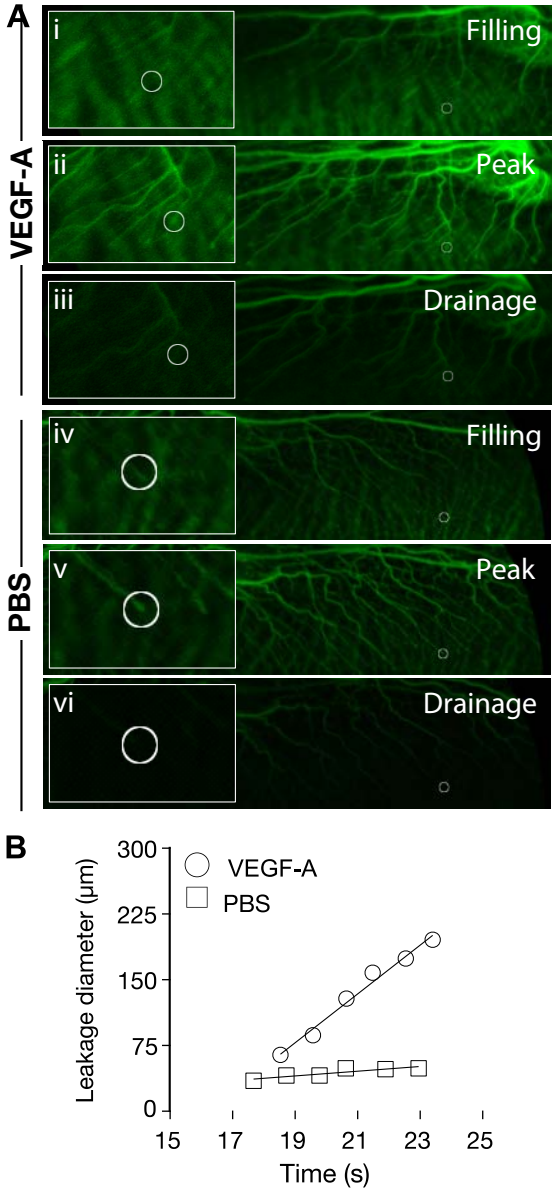

Figure 6. Localization of VEGF-A-induced leakage in the retina. Early-phase angiographies, 48 h after intraocular VEGF (100 ng) or PBS injections. *A*) Video frames show the fluorescence signal at the tips of retinal capillaries (○) . *i–iii*) Leakage occurred in the VEGF-A-injected eyes; insets show magnified views. *i*) Filling phase. Fluorescence in the choroid, the retinal arteries, but not yet in retinal capillaries (17.3 s postfluorescein). *ii*) Peak fluorescence. Both the retinal capillaries and the venules filled; the fluorescence in the choroid on the decline. Bubbles appear and begin to grow around the capillary tips (19.6 s). *iii*) Drainage phase. Signal mainly from retinal veins and gradually on the decline. Lack of fluorescence signal from the choroid. Although the capillaries are no longer filled with fluorescence, the fluorescence bubble around them is still present, expanding and rapidly fading away (23.4 s). *iv–vi*) Fluorescence in PBS-injected animals at the corresponding times. *iv*) Filling phase (17.5 s). *v*) Peak fluorescence (19.8 s). *vi*) Drainage phase (23.6 s). *B*) Quantification of the rates of leakage spreading in VEGF-injected (26±2 μm/s) and PBS-injected (3±1 μm/s) animals from linear regressions fitted to the measured data.

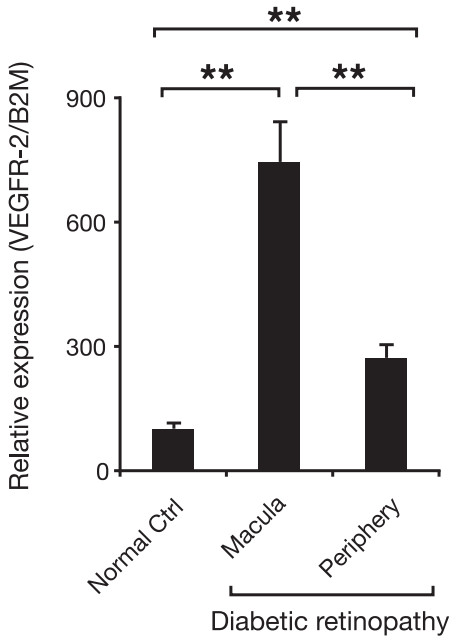

Figure 7. Increased VEGFR-2 in retinas of diabetic patients. Quantitative real-time RT-PCR analysis of VEGFR-2 in macular and peripheral retinal tissues from human diabetic samples (n=7, each group) and normal controls (n=5). The mRNA levels were normalized to 3 housekeeping genes, BACT, GAPDH, and B2M, the outcome of which were comparable. VEGFR-2 expression was increased in macula and periphery of diabetic samples, however, significantly more in the macula compared to the periphery.

In the diabetic retina, we found VEGFR-2 primarily in the capillaries compared to the larger vessels. Consistently, intravitreal injection of VEGF-A in the rabbit eye showed leakage at the tips of retinal capillaries. Since the proliferative DR is a microvascular disease, the expression and distribution of VEGFR-2 in diabetes suggest a mechanistic role for this molecule in the pathogenesis.

Our results show the translational potential of VEGFR-2 as a biomarker for DR. Molecular imaging of endothelial VEGFR-2 could provide a warning before clinical symptoms develop. At such an early stage, effective treatments could halt disease progression. Ultimately, whether VEGFR-2 can predict human DR will need to be decided in future clinical trials. FJ

This work was supported by the U.S. National Institutes of Health (NIH)/National Institute of Diabetes and Digestive and Kidney Diseases through Diabetes Complications Consortium award 25732-30, the BrightFocus Foundation, the Malaysian Palm Oil Board, National Natural Science Foundation of China grant 81171381, Heilongjiang overseas fund grant LC2011C27, NIH/National Eye Institute grant R01-EY019065 (Z.A.), an unrestricted grant of Research to Prevent Blindness to the Department of Ophthalmology at the Medical University of South Carolina,, and the South Carolina Lions Association. D.S., S.N., F.X., S.Z., A.B., M.R.K., S.S., Z.S.S., S.F., and Z.A. performed the research; D.S., S.N., Z.S.S., H.A., and A.H.-M. analyzed the data; and A.H.-M. wrote the paper. The authors declare no conflicts of interest.

REFERENCES

1. Sherwin, R., and Jastreboff, A. M. (2012) Year in diabetes 2012: the diabetes tsunami. *J. Clin. Endocrinol. Metab.* **97,** 4293–4301
2. Ishibashi, T., and Inomata, H. (1993) Ultrastructure of retinal vessels in diabetic patients. *Br. J. Ophthalmol.* **77,** 574–578
3. Lorenzi, M., and Gerhardinger, C. (2001) Early cellular and molecular changes induced by diabetes in the retina. *Diabetologia* **44,** 791–804
4. Ishibashi, T., Inomata, H., Sakamoto, T., and Ryan, S. J. (1995) Pericytes of newly formed vessels in experimental subretinal neovascularization. *Arch. Ophthalmol.* **113,** 227–231
5. Murakami, T., Suzuma, K., Takagi, H., Kita, M., Ohashi, H., Watanabe, D., Ojima, T., Kurimoto, M., Kimura, T., Sakamoto, A., Unoki, N., and Yoshimura, N. (2006) Time-lapse imaging of vitreoretinal angiogenesis originating from both quiescent and mature vessels in a novel ex vivo system. *Invest. Ophthalmol. Vis. Sci.* **47,** 5529–5536
6. Dvorak, H. F., Sioussat, T. M., Brown, L. F., Berse, B., Nagy, J. A., Sotrel, A., Manseau, E. J., Van de Water, L., and Senger, D. R. (1991) Distribution of vascular permeability factor (vascular endothelial growth factor) in tumors: concentration in tumor blood vessels. *J. Exp. Med.* **174,** 1275–1278
7. Hata, Y., Miura, M., Nakao, S., Kawahara, S., Kita, T., and Ishibashi, T. (2008) Antiangiogenic properties of fasudil, a potent Rho-Kinase inhibitor. *Jpn. J. Ophthalmol.* **52,** 16–23
8. Aiello, L. P., Avery, R. L., Arrigg, P. G., Keyt, B. A., Jampel, H. D., Shah, S. T., Pasquale, L. R., Thieme, H., Iwamoto, M. A., Park, J. E., Nguyen, H. V., Aiello, L. M., Ferrara, N., and King, G. L.(1994) Vascular endothelial growth factor in ocular fluid of patients with diabetic retinopathy and other retinal disorders. *N. Engl. J. Med.* **331,** 1480–1487
9. Jardeleza, M. S., and Miller, J. W. (2009) Review of anti-VEGF therapy in proliferative diabetic retinopathy. *Semin. Ophthalmol.* **24,** 87–92
10. Nakao, S., Zandi, S., Hata, Y., Kawahara, S., Arita, R., Schering, A., Sun, D., Melhorn, M. I., Ito, Y., Lara-Castillo, N., Ishibashi, T., and Hafezi-Moghadam, A. (2010) Blood vessel endothelial VEGFR-2 delays lymphangiogenesis: an endogenous trapping mechanism links lymph- and angiogenesis. *Blood* **117,** 1081–1090
11. Miyahara, S., Almulki, L., Noda, K., Nakazawa, T., Hisatomi, T., Nakao, S., Thomas, K. L., Schering, A., Zandi, S., Frimmel, S., Tayyari, F., Garland, R. C., Miller, J. W., Gragoudas, E. S., Masli, S., and Hafezi-Moghadam, A. (2008) In vivo imaging of endothelial injury in choriocapillaris during endotoxin-induced uveitis. *FASEB J.* **22,** 1973–1980
12. Sun, D., Nakao, S., Xie, F., Zandi, S., Schering, A., and Hafezi-Moghadam, A. (2010) Superior sensitivity of novel molecular imaging probe: simultaneously targeting two types of endothelial injury markers. *FASEB J.* **24,** 1532–1540
13. Xie, F., Sun, D., Schering, A., Nakao, S., Zandi, S., Liu, P., and Hafezi-Moghadam, A. (2010) Novel molecular imaging approach for subclinical detection of iritis and evaluation of therapeutic success. *Am. J. Pathol.* **177,** 39–48
14. Hafezi-Moghadam, A., Thomas, K. L., Prorock, A. J., Huo, Y., and Ley, K. (2001) L-selectin shedding regulates leukocyte recruitment. *J. Exp. Med.* **193,** 863–872
15. Garland, R. C., Sun, D., Zandi, S., Xie, F., Faez, S., Tayyari, F., Frimmel, S. A., Schering, A., Nakao, S., and Hafezi-Moghadam, A. (2011) Noninvasive molecular imaging reveals role of PAF in leukocyte-endothelial interaction in LPS-induced ocular vascular injury. *FASEB J.* **25,** 1284–1294
16. Frank, R. N. (2009) Treating diabetic retinopathy by inhibiting growth factor pathways. *Curr. Opin. Investig. Drugs* **10,** 327–335
17. Antonetti, D. A., Barber, A. J., Bronson, S. K., Freeman, W. M., Gardner, T. W., Jefferson, L. S., Kester, M., Kimball, S. R., Krady, J. K., LaNoue, K. F., Norbury, C. C., Quinn, P. G., Sandirasegarane, L., and Simpson, I. A. (2006) Diabetic retinopathy: seeing beyond glucose-induced microvascular disease. *Diabetes* **55,** 2401–2411
18. Noda, K., Melhorn, M. I., Zandi, S., Frimmel, S., Tayyari, F., Hisatomi, T., Almulki, L., Pronczuk, A., Hayes, K. C., and Hafezi-Moghadam, A. (2010) An animal model of spontaneous metabolic syndrome: Nile grass rat. *FASEB J.* **24,** 2443–2453
19. Noda, K., Nakao, S., Zandi, S., Sun, D., Hayes, K. C., and Hafezi-Moghadam, A. (2014) Retinopathy in a novel model of metabolic syndrome and type 2 diabetes: new insight on the inflammatory paradigm. *FASEB J.* **28,** 2038–2046
20. Hafezi-Moghadam, A., Thomas, K. L., and Cornelssen, C. (2004) A novel mouse-driven ex vivo flow chamber for the study of leukocyte and platelet function. *Am. J. Physiol. Cell. Physiol.* **286,** C876–892
21. Ikram, M. K., Cheung, C. Y., Lorenzi, M., Klein, R., Jones, T. L., and Wong, T. Y. (2013) Retinal vascular caliber as a biomarker for diabetes microvascular complications. *Diabetes Care* **36,** 750–759
22. Leenders, W., van Altena, M., Lubsen, N., Ruiter, D., and De Waal, R. (2001) In vivo activities of mutants of vascular endothelial growth factor (VEGF) with differential in vitro activities. *Int. J. Cancer* **91,** 327–333

Received for publication February 24, 2014.
Accepted for publication May 12, 2014.